nature communications

Article

https://doi.org/10.1038/s41467-024-52137-4

Enhanced continuous atmospheric water harvesting with scalable hygroscopic gel driven by natural sunlight and wind

Xinge Yang, Zhihui Chen, Chengjie Xiang, He Shan & Ruzhu Wang

Institute of Refrigeration and Cryogenics, MOE Engineering Research Center of Solar Power and Refrigeration, Shanghai Jiao Tong University, 200240, Shanghai, China.

Published on 03 September, 2024

Sonali
14.06.2025

Introduction

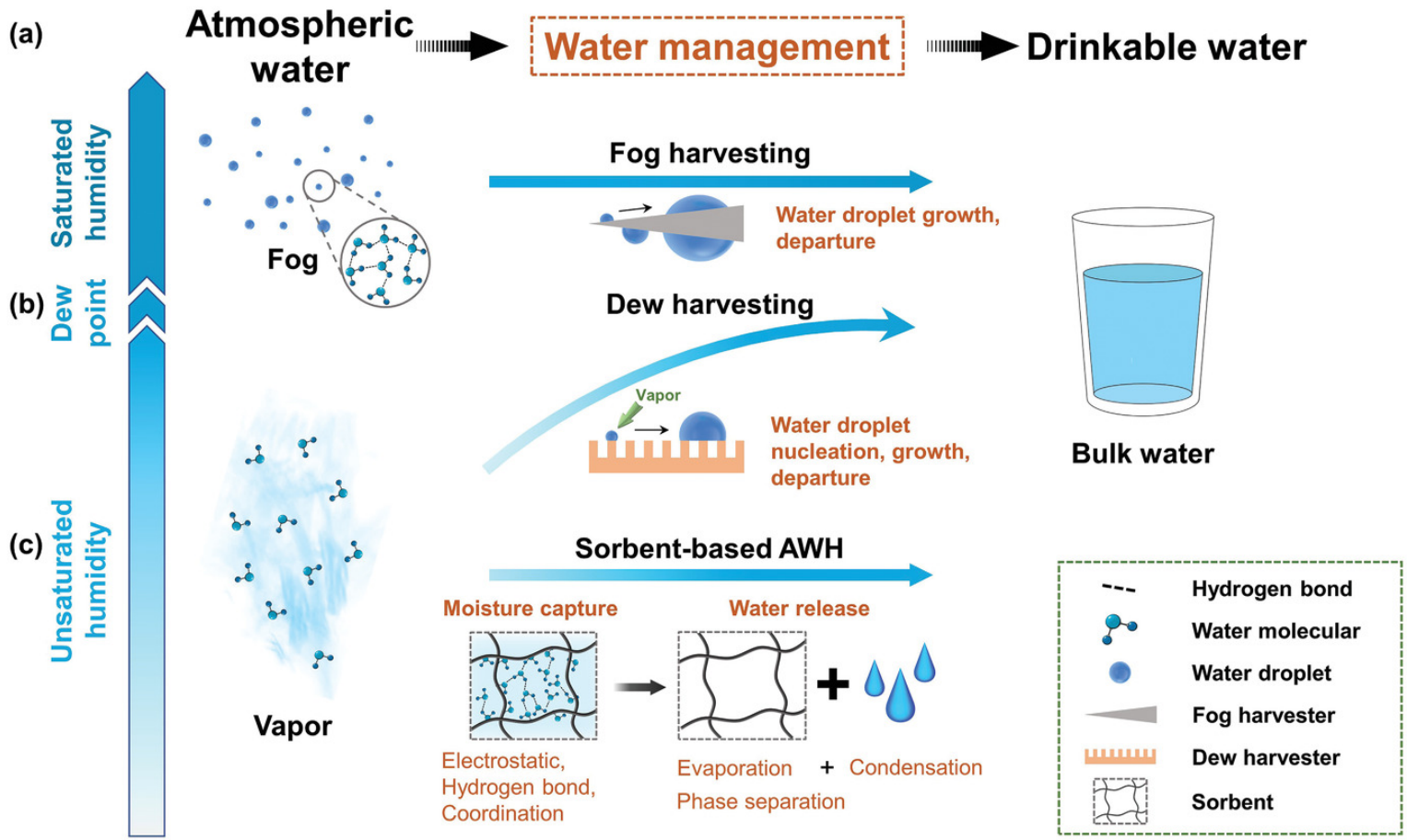

G. Yu, *et al.*, *Adv. Mater.*, **2022**, *34*, 2110079.

Background

MOF-based

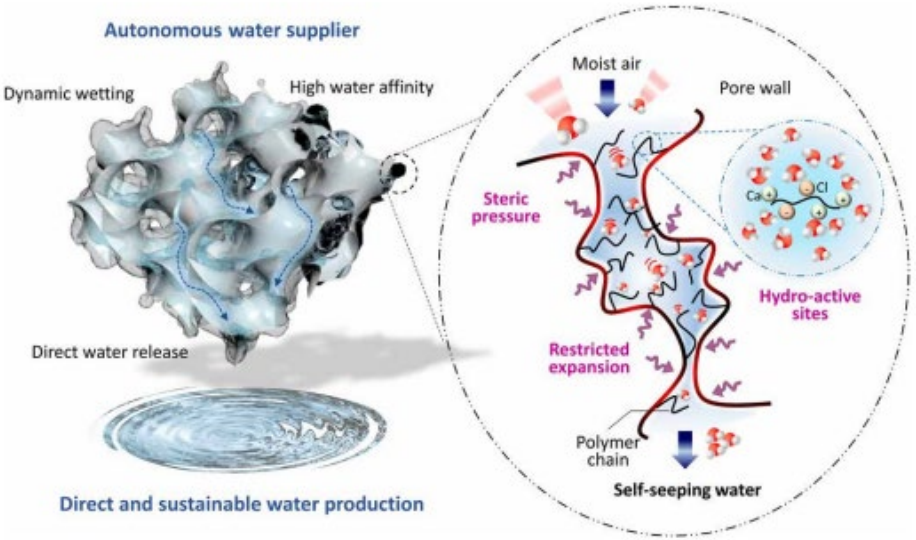

Polymer-based

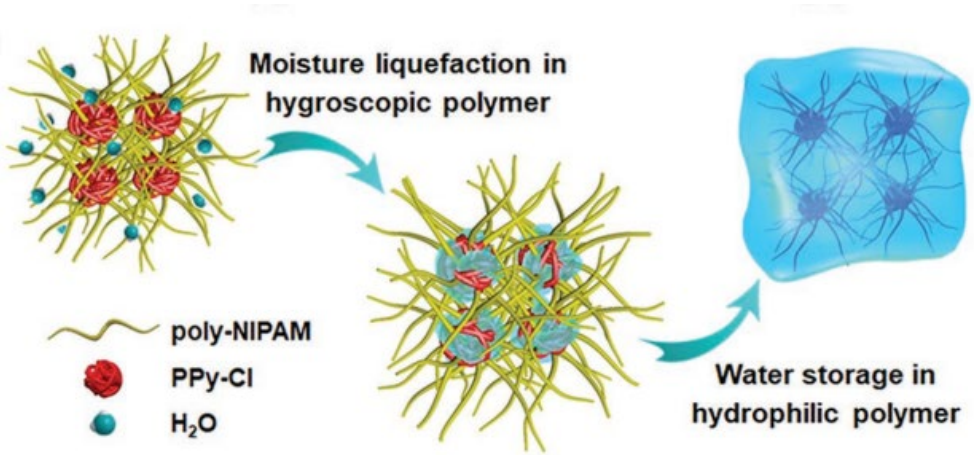

Salt-based

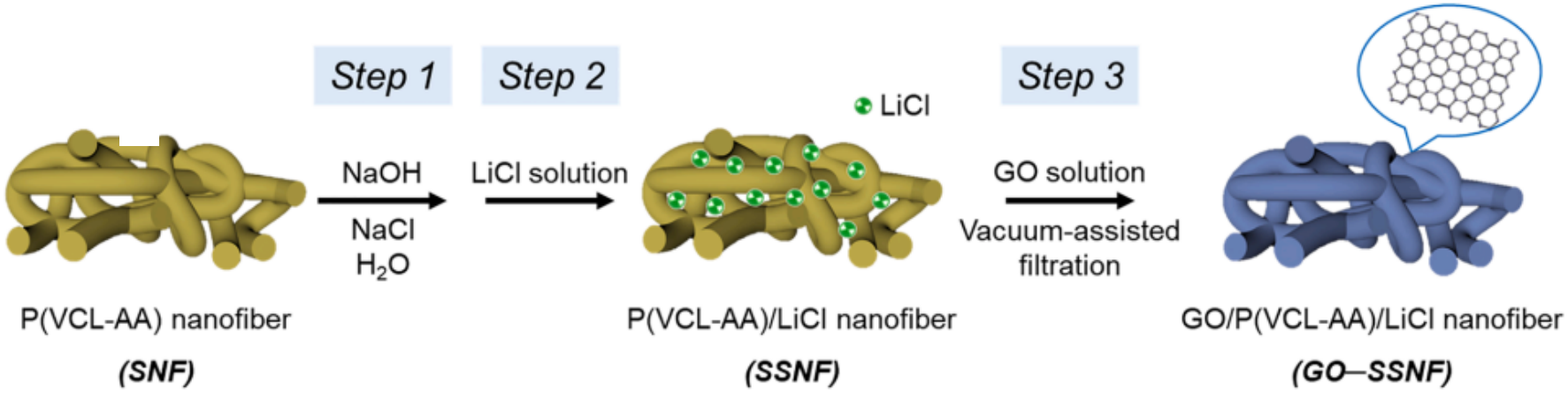

Yilmaz et al. *Sci. Adv.,*2020,**6,** 8605-8612.
Guihua Hu et al., *Adv. Mater.* 2019**, 31,** 1806446 -1806452.
S.Kim et al. *Chem.Eng.J.,*2021, **425,** 134601-131610.

Why this paper?

- A hygroscopic, interconnected polymeric gel is formed, exhibiting fast adsorption and desorption kinetics.
- High scalability and the stability of the composite.
- Quasi double-sided sorption, increasing contact area and sorption rate.
- Here, one part absorbs vapours while the other part releases vapours.

HIPG

- Hydroxypropyl methyl cellulose
- Sodium polyacrylate
- LiCl and TiN nanoparticles

Introduction: Synthesis of HIPG

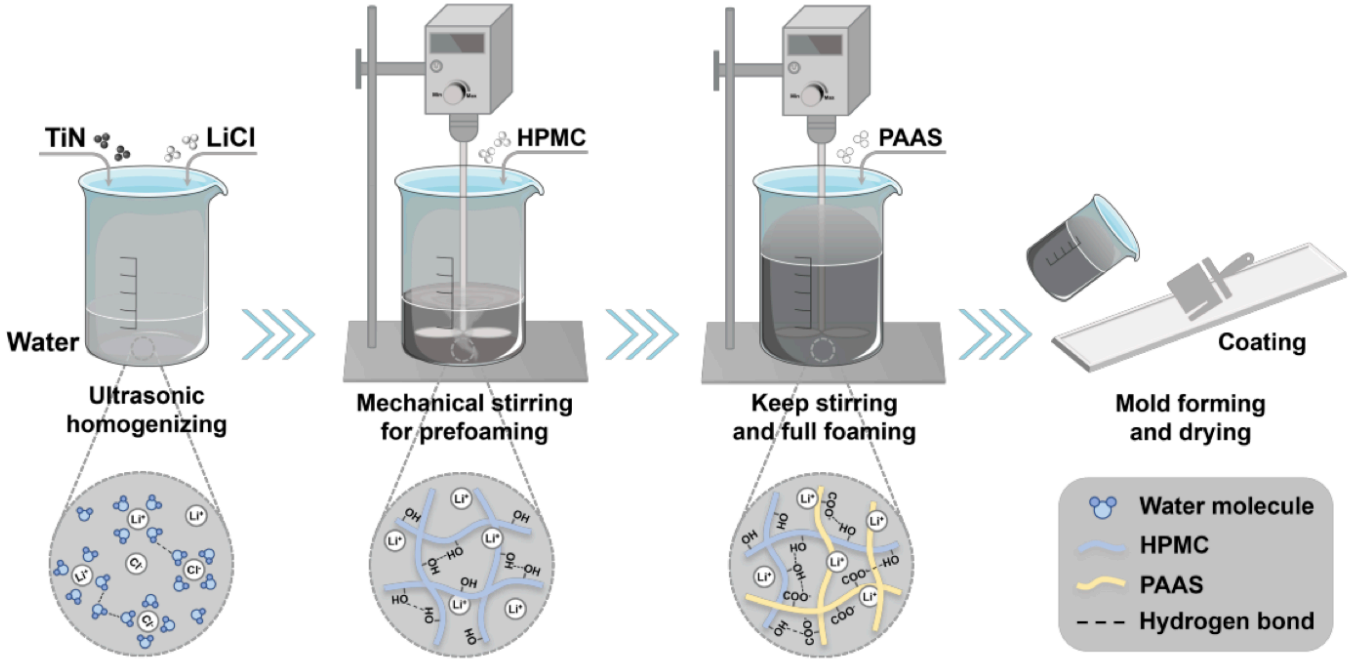

Supplementary Fig. 5 | Scheme of the synthesis process and mechanism of HIPG. (Beaker-gray icon by Servier https://smart.servier.com/ is licensed under CC-BY 3.0 Unported https://creativecommons.org/licenses/by/3.0/. The color of the "solution in the beaker" changed from light gray to dark gray and the height of the "solution" also changed. The "white label and bubbles in the solution" were deleted.)

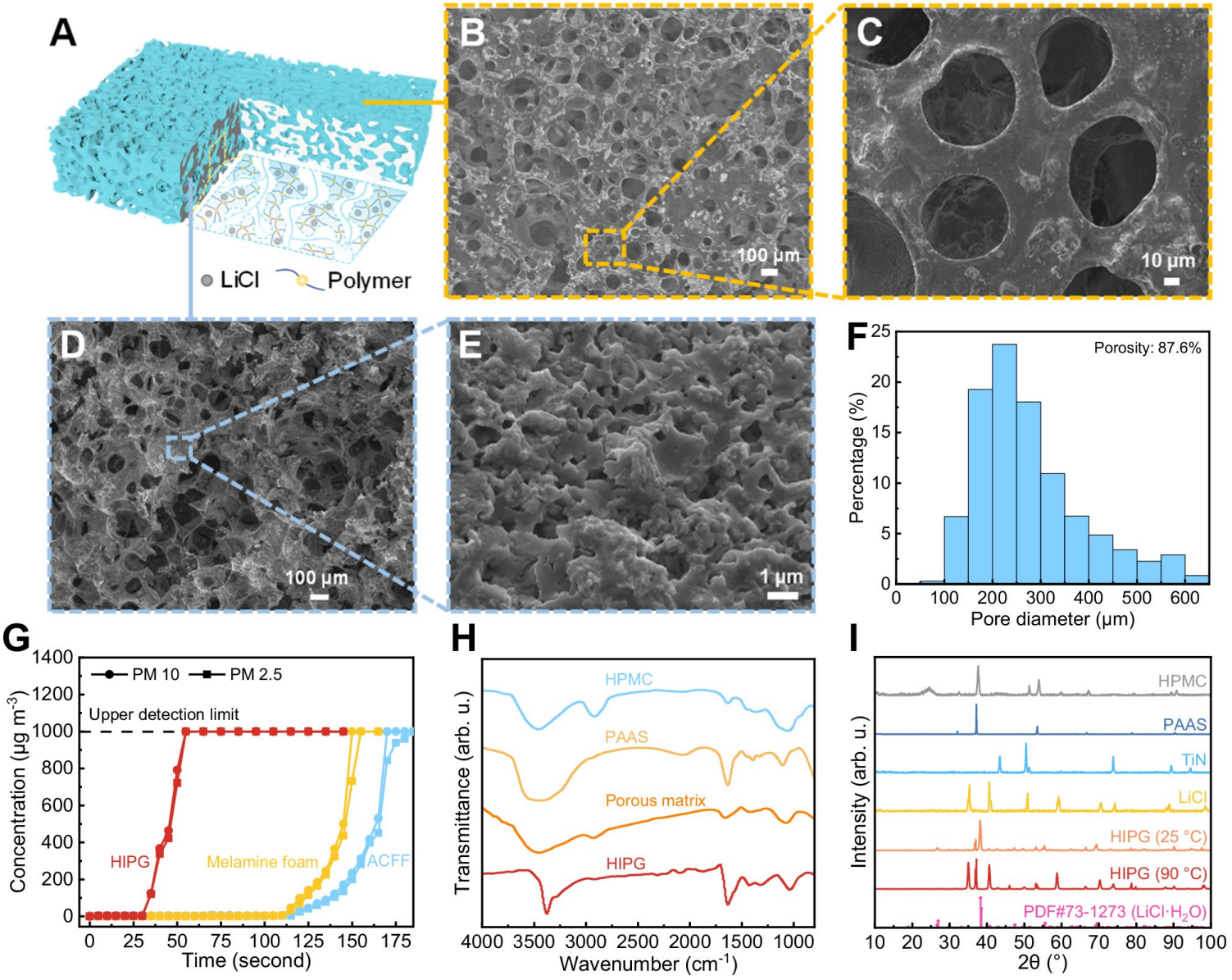

A The schematic of the structure of HIPG and the water vapor transport within the HIPG. **B**, **C** The SEM images of HIPG from the top view (**B**) and high magnification (**C**). **D**, **E** The SEM images of HIPG from the cross-sectional view (**D**) and high magnification (**E**). **F** The pore size distribution of HIPG. **G** The concentration changes of $PM_{2.5}$ and PM_{10} detected by the detectors located in the receiving cavity for different porous matrixes over time. **H** The FTIR patterns of HIPG at ~23 °C, ~60% RH. **I** The XRD patterns of each component and HIPG at different temperatures.

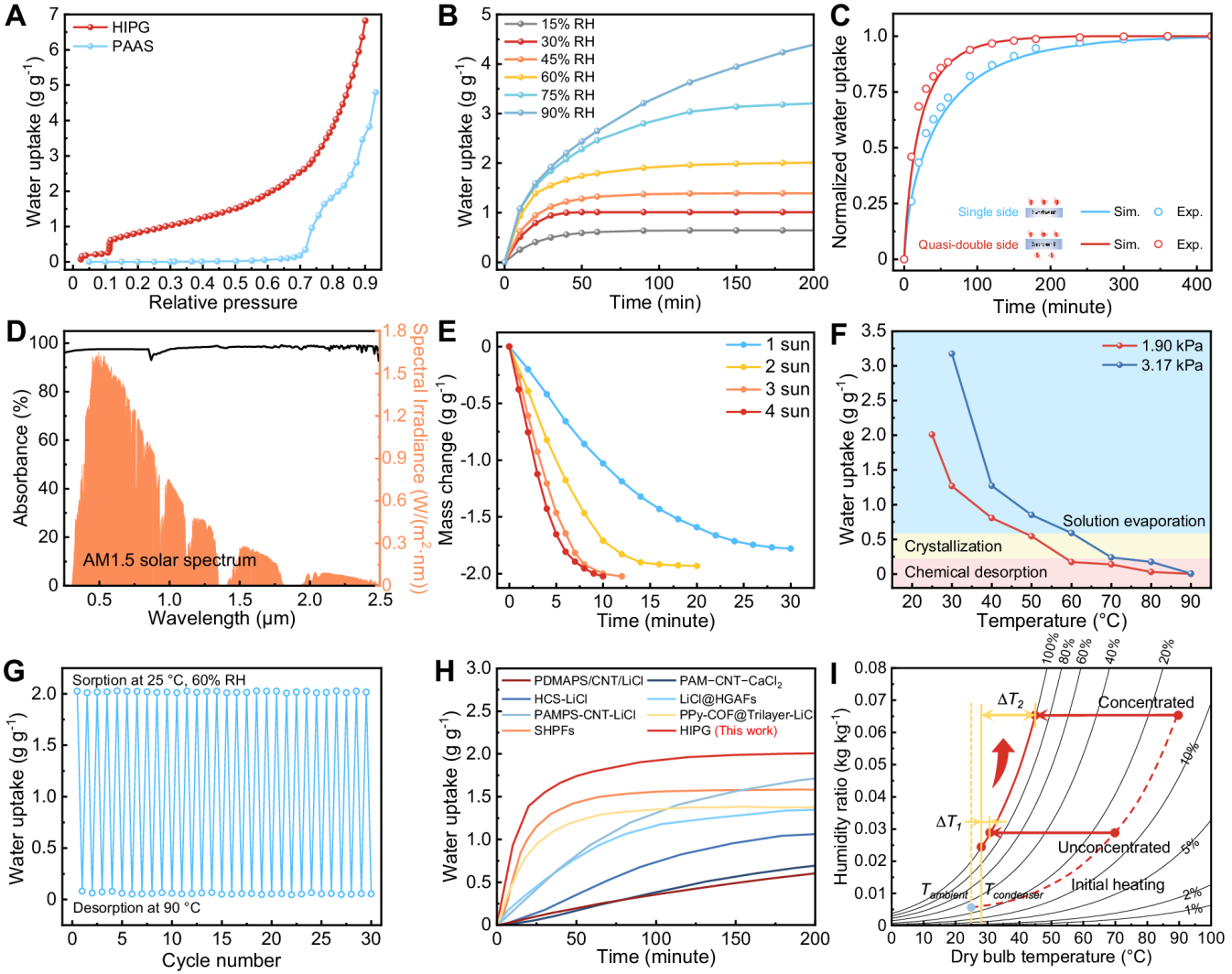

A The water sorption isotherms of HIPG and PAAS at 25 °C. **B** The dynamic water sorption processes of bulk HIPG at the same temperature of 25 °C and different RHs of 30%, 45%, 60%, 75%, and 90%. **C** The experimental and simulated results of dynamic sorption processes for the single-sided sorption and quasi-double-sided sorption under 25 °C and 60% RH. The water uptake was normalized by dividing the equilibrium sorption capacity. **D** The UV–vis–NIR absorption spectrum of HIPG. **E** The solar-driven desorption processes of HIPG with sorption equilibrium at 25 °C, 60% RH under the same ambient temperature and RH and different solar irradiation intensities. **F** The water desorption isobars of HIPG at water vapor pressure of 1.90 and 3.17 kPa. **G** Thirty water sorption–desorption cycling tests of HIPG at 25 °C, 60% RH (1.90 kPa) for sorption and 90 °C, 4.2% RH (3.17 kPa) for desorption. **H** The comparison of water sorption performances of bulk HIPG and other state-of-the-art salt-based composite sorbents[20,24,29,31,44,48,49]. **I** Psychrometric chart showing the water desorption-condensation processes for the continuous SAWH device with and without solar concentration.

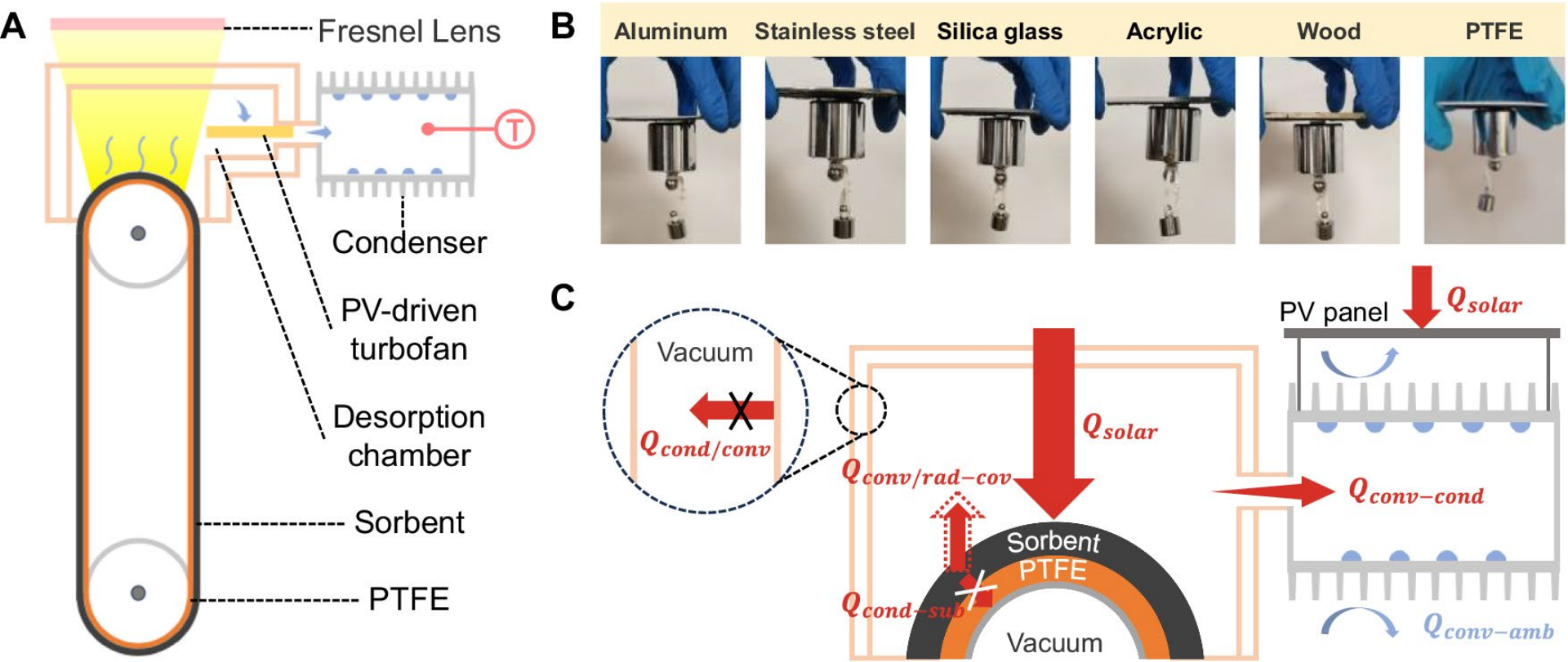

A The structure schematic of the continuous SAWH device. **B** The adhesion properties of HIPG on various substrates, including aluminium, stainless steel, silica glass, acrylic, wood, and PTFE (weight: the big one: 100 g; the small one: 20 g). **C** The heat transfer analysis of the continuous SAWH device during the desorption-condensation processes.

The HIPG-coated conveyor belt allows air contact on both sides, enhancing the sorption

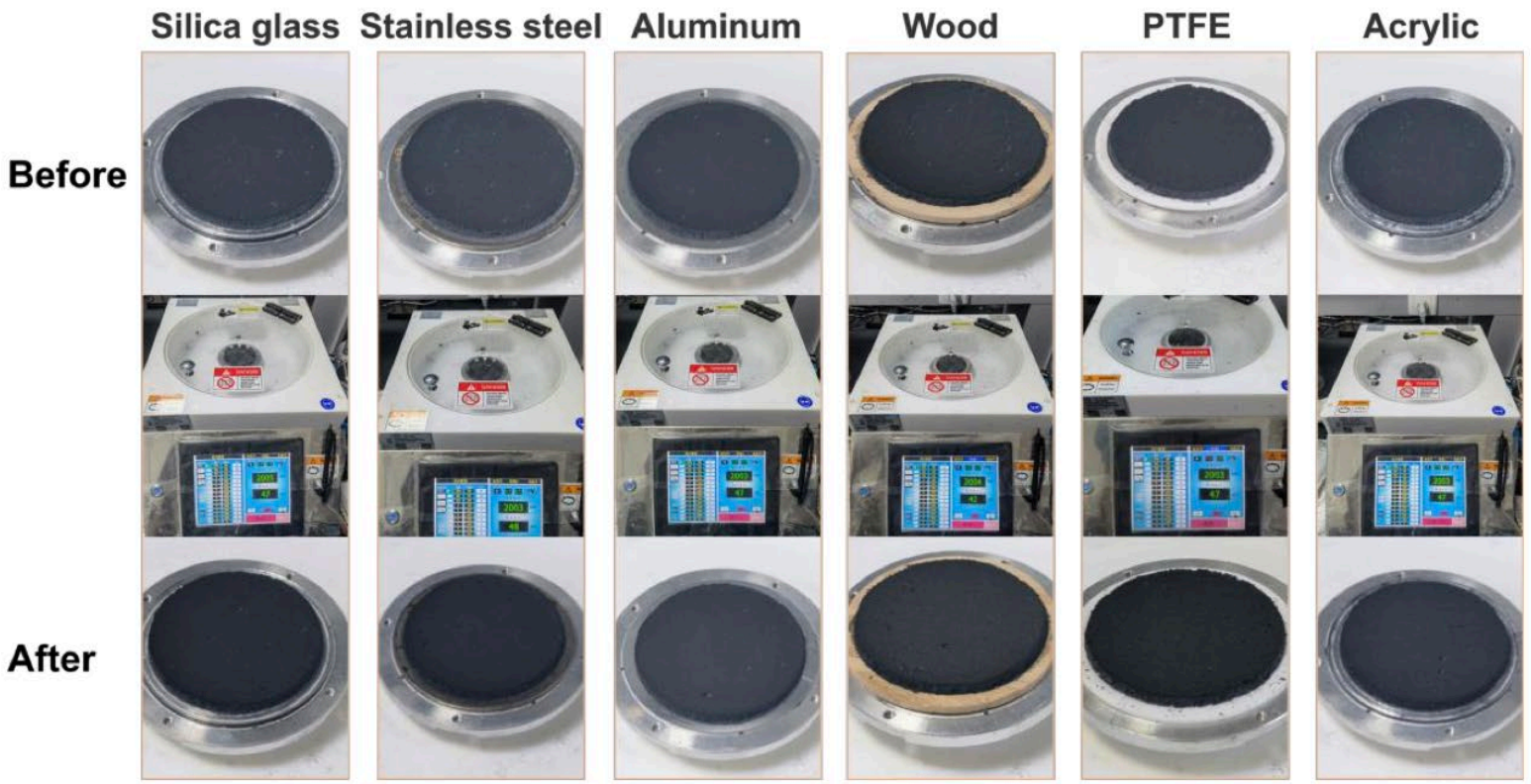

Supplementary Fig. 20 | The adhesion properties of dry HIPG on different substrates containing silica glass, stainless steel, aluminum, wood, PTFE, and acrylic under a rotation speed of 2000 rpm. The dry HIPGs could rotate at a high speed of 2000 rpm for one minute and still tightly adhered to the substrate with no deformation or damage.

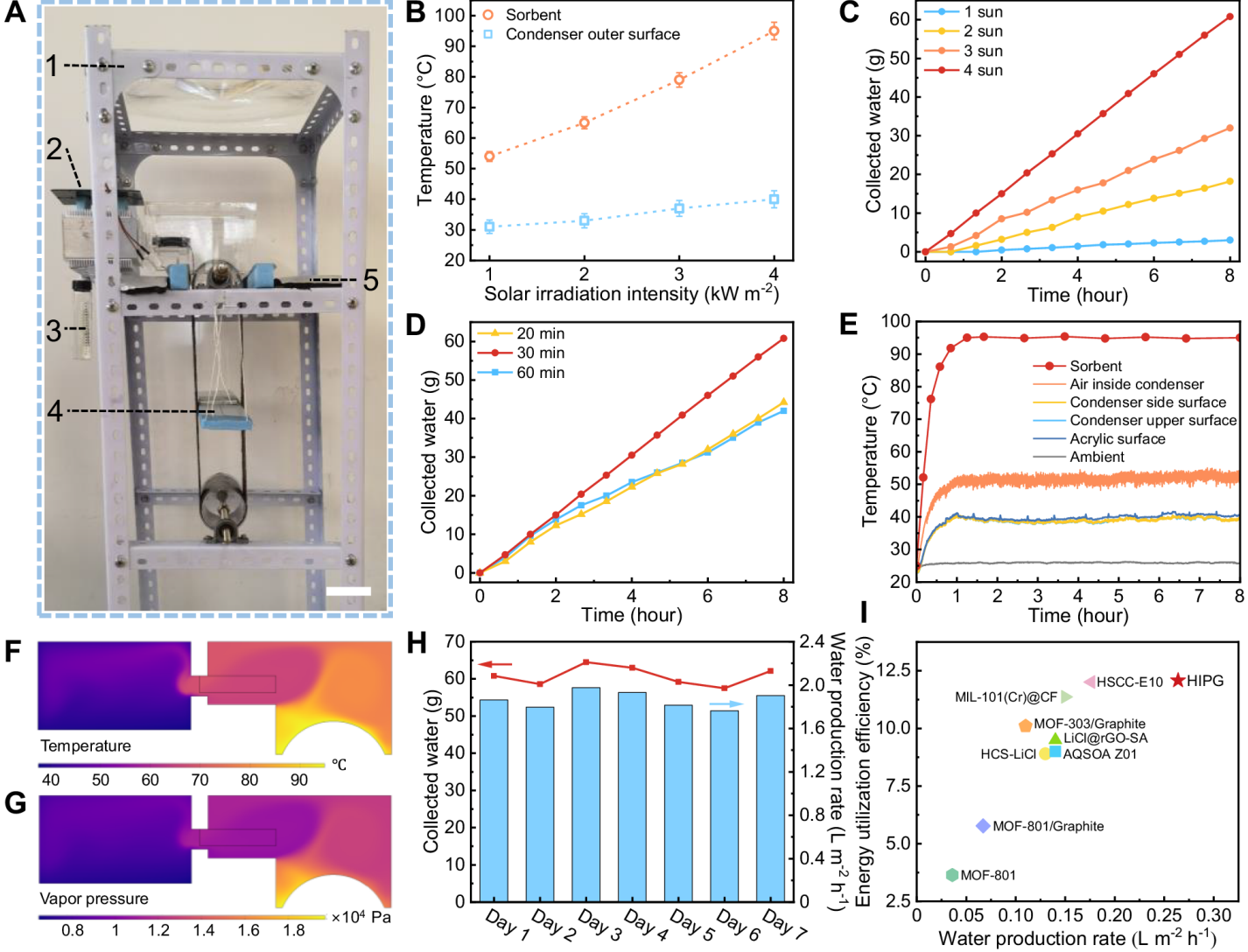

A The digital photo of the continuous SAWH device. 1-support frame, 2-PV panel, 3-water collector, 4-shading panel, 5-shading cotton. Scale length: 5 cm. **B**The temperature of the sorbent and condenser outer surface after reaching the thermal equilibrium during the water production tests under different solar intensities. Error bar: standard deviation (SD). **C** The mass changes of the collected water under different solar irradiation intensities over 8-hour indoor tests. **D** The mass changes of the collected water with different cycle times under 4 suns over 8-hour indoor tests. **E** The temperature evolutions of different positions of the continuous SAWH device with a cycle time of 30 minutes under 4 suns during the 8-hour indoor test. **F** and **G** The simulation results of the water desorption-condensation processes. The temperature (**F**) and water vapor partial pressure (**G**) distributions in the device. **H** The water yield and water production rate of the continuous SAWH device under 4 suns over seven-day cycles. **I** Water collection performance comparison of our work and other solar-driven SAWH device

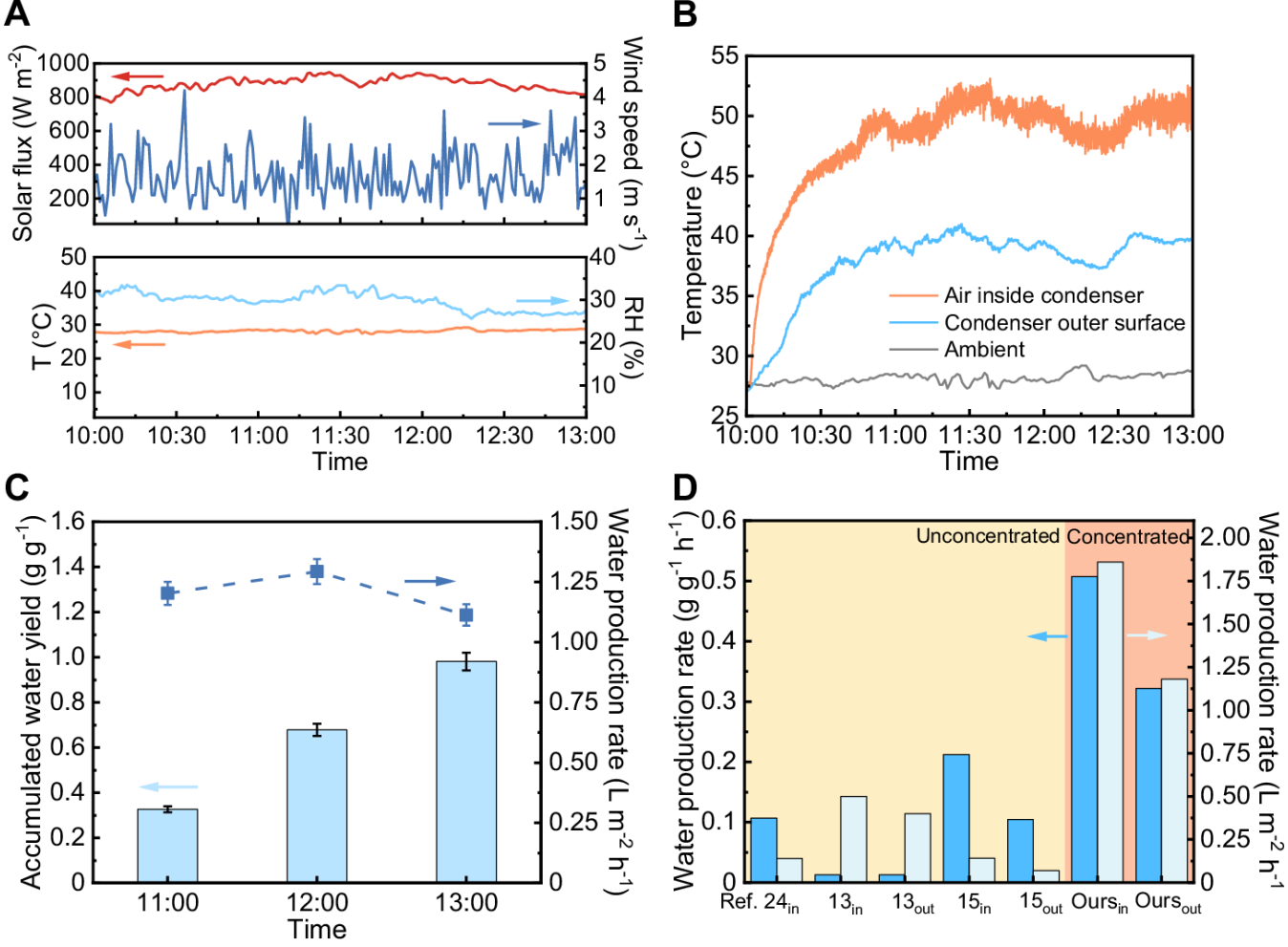

A The evolutions of natural solar irradiation intensity (without concentration), wind speed, ambient temperature, and RH over the 3-hour outdoor test. **B** The temperature evolutions of the air inside condenser, the condenser outer surface, and the environment during the 3-hour outdoor test. **C** The accumulated specific water yield and water production rate over the 3-hour outdoor test. Error bar: SD. **D** The comparison of water production rate of our continuous SAWH device and other previously reported state-of-the-art solar-driven continuous SAWH device

Conclusions

- Scalable strategy to develop HIPG with fast adsorption-desorption kinetics and strong adhesion properties.

- Enhanced water desorption and condensation.

- Wind energy was directly converted to mechanical motion to drive the moment of the sorption bed in the device.

- The device delivered 4050 $ml_{water/}kg_{adsorbent}$/day.

- 14.9 L water m^{-2} day^{-1} and thermal efficiency as high as 25.7% in indoor experiments (~57% RH) and 3.5–8.9 L water m^{-2} day^{-1} in outdoor experiments by solar concentration without any other energy consumption superior to the previous SAWH devices.